Applied Catalysis B: Environmental 138–139 (2013) 184–190

Contents lists available at SciVerse ScienceDirect

Applied Catalysis B: Environmental

journal homepage: www.elsevier.com/locate/apcatb

Ion-exchange synthesis and enhanced visible-light photocatalytic activities of CuSe-ZnSe flower-like nanocomposites

Weidong Shi*, Jiaqi Shi, Shuai Yu, Pei Liu

School of Chemistry and Chemical Engineering, Jiangsu University, Xuefu Road 301, Zhenjiang, 212013, PR China

ARTICLE INFO

Article history:
Received 27 November 2012
Received in revised form 19 January 2013
Accepted 3 February 2013
Available online 6 March 2013

Keywords:
CuSe-ZnSe nanocomposites
Ion-exchange reaction
Visible-light-driven
Photocatalytic activities
Organic dyes

ABSTRACT

CuSe-ZnSe flower-like nanocomposites with uniform diameters can be easily fabricated on a large scale by a controlled ion-exchange reaction between monodisperse ZnSe flower-like nanostructures and Cu^{2+} ions in solution. The difference of solubility products (K_{sp}) of ZnSe and CuSe is the main driving force for the formation of these flower-like nanocomposites. The Cu content greatly influences the physical properties and photocatalytic activity of obtained CuSe-ZnSe nanocomposites. The as-produced CuSe-ZnSe nanocomposites show tremendous enhancements on the photocatalytic degradation ratio of organic dyes methylene orange (MO) and methylene blue (MB) under visible-light irradiation. The 8 wt.% CuSe-ZnSe sample exhibits the highest degradation ratio for both MO (ca. 100%, 90 min) and MB (ca. 96%, 60 min), which are over 4 times and 2.5 times than that of the pure ZnSe sample, respectively. Based on the data of UV–vis diffuse reflection spectra, XPS and PL spectra, the enhancements of photocatalytic activities of CuSe-ZnSe flower-like nanocomposites are due to the effective separation of photo-electrons and holes induces by the direct initiates interfacial charge transfer (IFCT) from the valence band (VB) of ZnSe to CuSe, which results in the reduction of CuSe to Cu_2Se. This work not only highlights the potential use of visible-light-driven CuSe-ZnSe flower-like nanocomposites photocatalysts, but also emphasizes the simple ion-exchange in situ growth method for the preparation of selenides heterogeneous structures.

1. Introduction

In the past few decades, semiconductor photocatalysts have attracted considerable attention for a long time in the field of photochemistry due to their catalytic activity and broad applications in solving environmental problems. [1] Generally, they are used in the photocatalytic degradation of polluted wastewater. [2–5] It is well known that the semiconductor TiO_2 has been demonstrated to be a commonly used photocatalyst. However, its photocatalytic activity is often limited by its fast charge-carrier recombination and low interfacial charge-transfer rates of photogenerated carriers. Furthermore, because of its large band gap (3.2 eV for anatase and 3.0 eV for rutile), the photocatalyst can only absorb the UV light, which accounts for only 3–5% of the total sunlight that can reach the earth, and strongly restricts its practical applications. [6,7] Therefore, the development of new visible-light-responsive photocatalysts with high activities is currently an intensive and hot research topic.

As one of the important II–VI semiconductors, Zinc selenide (ZnSe) has been considered to be a prospective optical material due to its wide gap energy of 2.7 eV and large excitation binding energy of 21 meV. [8–11] Recently, the photocatalytic activities of ZnSe materials, especially nanostructures, have received much attention. [12–19] Studies show that almost reported ZnSe structures can only exhibit their good photocatalytic activities under UV light irradiation, although they possess the absorbing edge for visible light. Zhang et al. explored the photocatalytic activities of ZnSe flower-like hierarchical structures for the degradation of methyl orange (MO) dye under visible light irradiation. [16] But their efficiency is so low that the MO dye completely disappears after irradiating for about 9 h. In this regard, the strategies on the chemical modifications of a UV-active photocatalyst, including loading a noble metal, doping with a nonmetal and metal, surface sensitization, and a combination with various narrow band gap semiconductors, such as CdS, CuS, Fe_2O_3 and WO_3, can be often employed. [20–23] Among them, the composite of two semiconductors have been proved to extend strongly the absorption range and enhance the absorption of the solar spectrum. In addition, compared with a single semiconductor, composite semiconductors can promote the generation and separation of photo-induced electrons and holes, and so improve the photocatalytic efficiency dramatically.

* Corresponding author. Tel.: +86 51188791800.
E-mail address: swd1978@ujs.edu.cn (W. Shi).

0926-3373/$ – see front matter © 2013 Elsevier B.V. All rights reserved.
http://dx.doi.org/10.1016/j.apcatb.2013.02.031

[21] Very recently, nitrogen-doped graphene/ZnSe nanocomposites have been fabricated successfully by Yu et al. [24] It is found that the as-prepared composites exhibit enhanced photocatalytic activities for the degradation of MO dye under visible-light irradiation, compared with ZnSe commercial powder. But their efficiency is still relatively low (the degradation ratio of 71.5%, 7 h). In addition, the preparation procedures of these composites are also very complicated, which limits their further studies. Therefore, designing a simply synthetic route for more efficient visible-light-driven ZnSe-based composite photocatalytic materials is highly desirable.

Copper selenide (CuSe), as an important semiconductor, has been widely used in solar cell, optical filter, thermoelectric and photoelectric transformers and superconductors due to its complex structure and valence state. [25–31] It possesses the band gap of 2.15 eV, exhibiting excellent visible-light activity. [32] So we expect that coupling CuSe with ZnSe might be a promising visible-light active photocatalyst through utilizing p-n junction effect and band gap engineering. Until now, CuSe nanostructures with various morphologies, such as nanoplates, nanowires, nanocubes and nanodiscs, have been prepared by different methods. [33–37] It is very difficult to fabricate directly high-quality CuSe-ZnSe nanocomposites by using these above methods based on the homogeneous nucleation and growth mechanism. Ion-exchange approaches have been applied in the synthesis of many hetero-system nanocomposites, typically CuS-ZnS nanosheets, exhibiting many obvious advantages, such as low cost, convenient manipulation, excellent control over depositing proportion, and high contact extent between composite phases. [38–42] To the best of our knowledge, there is no report on the fabrication of CuSe-ZnSe nanocomposites by ZnSe as a precursor by ion-exchange approach and their visible-light photocatalytic activities.

Herein, we report for the first time the ion-exchange fabrication of high-quality CuSe-ZnSe flower-like nanocomposites. The CuSe amount is crucial in determining the visible-light photocatalytic activities of these nanocomposites for methylene orange (MO) and methylene blue (MB) dye. Especially, 8 wt.% CuSe-ZnSe sample exhibits the remarkably enhanced photocatalytic activities (ca. 100%) of MO dye for 1.5 h, which is over 4 times of that (ca. 25%) of pure ZnSe sample. The possible mechanism for the photo-degradation of dye on CuSe-ZnSe flower-like nanocomposites photocatalysts was also discussed.

2. Experimental

2.1. Sample preparation

All chemicals used in this experiment were of analytical grade. For the ZnSe flower-like nanostructure precursors (Sample 1), 14 mmol of NaOH was dissolved in 14 mL of distilled water and then 0.35 mmol of $Zn(NO_3)_2{\cdot}6H_2O$ and 3 mmol of ethylenediaminetetraacetic acid (EDTA) were added successively into the above solution. The resulting mixture was sonicated until a clear solution was obtained. Afterward, 0.34 mmol of Na_2SeO_3 and 7 mL of hydrazine hydrate $N_2H_4{\cdot}H_2O$ (85%) were sequentially added into this reaction. After the mixture was magnetic stirred for 10 min, the final solution was then transferred into a Teflon-lined autoclave of 50 mL capacity. After heating at 180 °C for 2 h, the tank was cooled down to room temperature naturally. Large quantities of yellowish floccules of well-crystallized ZnSe flower-like nanostructure were formed by treatment of the reaction with 1 M HCl solution.

For the CuSe-ZnSe flower-like nanocomposites, the as-obtained ZnSe precursors (ca. 0.03 g) were washed with distilled water for several times, and added into the of $CuCl_2$ aqueous solution. The samples 2–4 were obtained in the different concentration (1 wt.%, 3 wt.% and 8 wt.%) of $CuCl_2$ aqueous solution. Final samples were dried under vacuum at 60 °C for 2 h.

2.2. Characterization and measurements

The X-ray diffraction pattern of the products was collected on a Rigaku-D/max 2500 V X-ray diffractometer with Cu Kα radiation (λ = 1.5418 Å), with an operation voltage and current maintained at 40 kV and 40 mA. The samples were prepared by sonicating powdered samples in ethanol and then evaporating one drop of the suspension on a glass slide. The morphology and size of the samples were characterized by scanning electron microscopy (SEM, Nova 400 Nano) and transmission electron microscopy (TEM, TECNAI20, Philips). The absorption spectrum was carried out in the wavelength range of 240–800 nm using a computer aided double-beam spectrophotometer (UV-VIS-NIR, Hitachi U-4100). X-ray photoelectron spectra (XPS) were recorded on an ESCALAB MK II X-ray photoelectron spectrometer using nonmonochromatized Al-Mg KR radiation exciting source. Photoluminescence spectra were recorded on a Shimadzu RF-5301 spectrophotometer.

2.3. Photocatalytic degradation of organic dye

The photo-degradation of MO and MB dyes was carried out at 308 K in a photochemical reactor under visible light. The photochemical reactor contains 30 mg CuSe-ZnSe flower-like nanocomposites and 1.0×10^{-4} M of 100 mL MO or MB solution. To exclude the influence of physical adsorption, the reactor was kept into darkness for 30 min to reach the adsorption equilibrium. The photochemical reactor was irradiated with a 300 W Xenon lamp which was located with a distance of 8 cm at one side of the containing solution. UV lights with wavelengths less than 420 nm were removed by a UV-cutoff filter. The sampling analysis was conducted in 10 min interval. The photocatalytic degradation ratio (*DR*) was calculated by the following formula:

$$DR = \left(1 - \frac{A_i}{A_0}\right) \times 100\%$$

A_0 is the initial absorbency of MO or MB that reached absorption equilibrium, while A_i is the absorbency after the sampling analysis. At given irradiation time, a series of aqueous solutions in a certain volume were collected and filtered through a Millipore filter for analysis. The absorption spectrum of the filtrate was measured on a Hitachi U-4100 spectrophotometer. The concentration of dye was determined by monitoring the changes in the main absorbance centered at 465 nm for MO or 656 nm for MB.

3. Results and discussion

The phase purity of as-obtained ZnSe nanoflowers were characterized by XRD, and the pattern is shown in Fig. 1. All the peaks in the pattern can be readily indexed to a cubic-phase ZnSe (space group *F*-43*m* (2 1 6)) with lattice constants *a* = 5.669 Å (JPCDS card No. 37-1463). No peaks of other impurities can be detected, which indicates that the samples are pure phase. The morphology of the typical samples prepared by the procedure described in Section 2 are visualized by SEM, as shown in Fig. 1b and c. At lower magnification, the SEM image (Fig. 1b) reveals that the ZnSe samples consist almost entirely of 3D flowerlike structures with a diameter of ca. 2–4 μm and a relatively narrow size distribution. The yield of these 3D structures is very high (above 98%). The high magnification SEM image (Fig. 1c) reveals that the thickness of a leaf in the 3D flower-like structures is quite thin (ca. 30 nm). The chemical composition of these nanoflowers is further characterized by using EDS (Fig. 1d). Besides the element Au and Si, from the substrate, only peaks of the

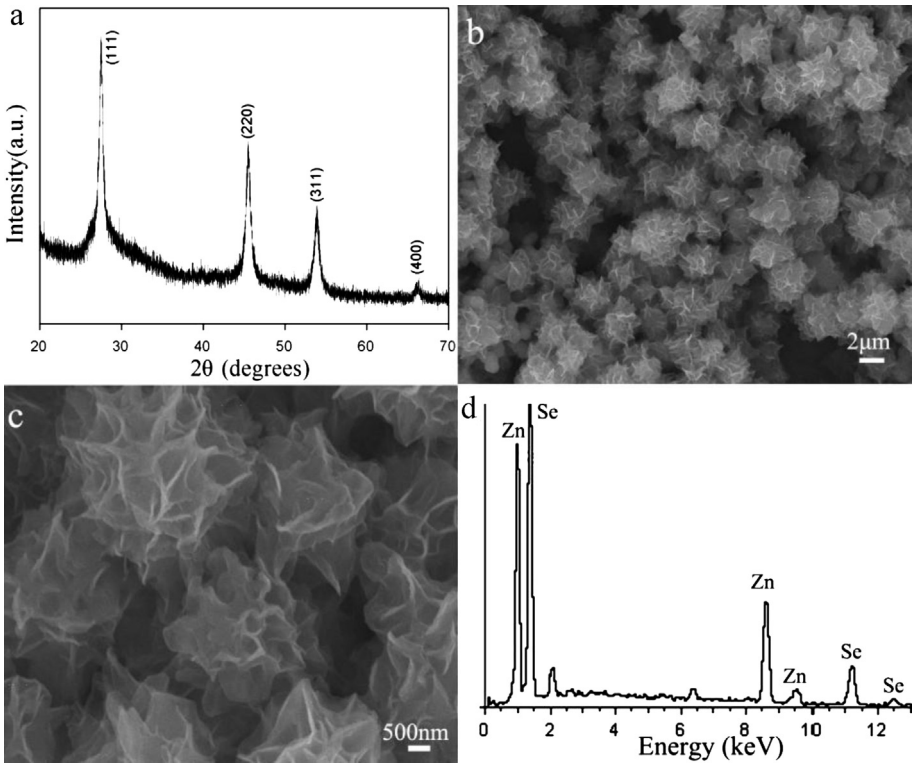

Fig. 1. Characterization of as-obtained pure ZnSe nanoflowers (sample 1): (a) XRD pattern, (b) low-magnification SEM image, (c) high-magnification SEM image and (d) EDS pattern.

elements Zn and Se are detected in the EDS pattern and the molar ratio is ca. 1: 1.

The synthesis of CuSe-ZnSe flower-like nanocomposites were preformed by a simple ion-exchange reaction between Cu^{2+} ions and the above-prepared monodisperse ZnSe flower-like nanostructures. Fig. 2 shows the XRD pattern of the CuSe-ZnSe composites (sample 2–4) obtained in the different concentration of $CuCl_2$ aqueous solution. It can be seen that both ZnSe and CuSe are indentified in these samples according to their standard diffraction peaks. The peaks of the CuSe phase in the XRD pattern can be assigned to hexagonal phase CuSe (space group P63/mmc(194)) with lattice constants of $a = 3.984$ Å and $c = 17.288$ Å, which are in good agreement with the literature values (JCPDS 27-0185). The broadening of the diffraction peaks is caused by the small crystallite size, which is estimated to be ca. 22.3 nm. Furthermore, with increasing the amount of added Cu^{2+} ions in the reaction system, the ratio of the peak intensity at 27.8° from CuSe to that at 27.2° from ZnSe can be also found to increase correspondingly in the XRD patterns of samples 2–4. This indicates the CuSe content of the as-obtained flower-like nanocomposites can be easily controlled. The elemental compositions of sample 4 were further analyzed by XPS (Fig. 3). As shown in Fig. 3b, the BEs of Cu $2p_{3/2}$ and Cu $2p_{1/2}$ peaks are at 932.9 and 952.8 eV, respectively. A weak peak at 943.5 eV corresponding to the satellite peak of Cu^{2+} can be also observed in this pattern. The symmetrical shapes of the two Cu 2p peaks show the presence of pure CuSe. Fig. 3c exhibits the BEs of Zn $2p_{3/2}$ and Zn $2p_{1/2}$ can be assigned to the two strong peaks at 1022.3 and 1045.2 eV, respectively. Compared with Zn 2p XPS peaks of pure ZnSe, a slight shift for that of sample 4 can be observed due to the electronic exchange at the interfaces from Zn to Cu caused by their electronegativity difference. [43] In addition, the slight shift of the Se 2p peak at 53.8 eV for sample 4 also indicates the presence of composite metal selenides (Fig. 3d). Chemical analysis of single flower-like nanocomposite (sample 4) was further confirmed by electron energy loss spectroscopy (EEELS, Fig. 4). The elements Cu, Zn, Se are homogeneously distributed throughout the nanocomposite, which proves that the in situ and uniform growth of CuSe clusters on the surface of ZnSe flower-like nanostructures can be realized well by this simple ion-exchange reaction.

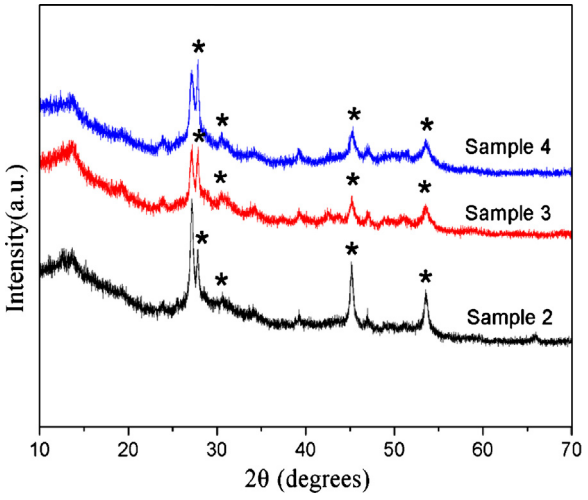

Fig. 2. XRD patterns of sample 2, 3 and 4. The peaks marked with an asterisk (*) from CuSe phase.

On the basis of the above evolution experiments of the concentration-dependent phase structures and the final morphology of samples, it is believed that the difference of solubility products (K_{sp}) of ZnSe ($10^{-29.4}$) and CuSe ($10^{-48.1}$) is the main driving force for the formation of CuSe-ZnSe flower-like nanocomposites. There are two main chemical reactions existing during the above-mentioned phase evolution:

$$ZnSe \rightarrow Zn^{2+} + Se^{2-} \quad (1)$$

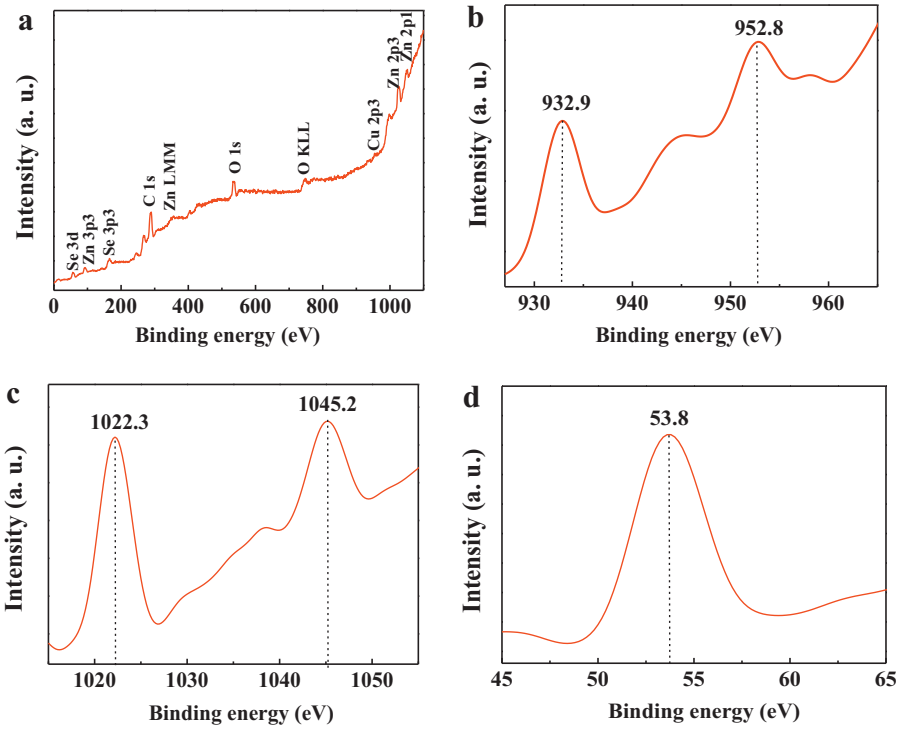

Fig. 3. Typical XPS analysis of sample 4: (a) survey spectrum, (b) copper region, (c) zinc region and (d) selenium region.

$$Cu^{2+} + Se^{2-} \rightarrow CuSe \quad (2)$$

There are a few amounts of Se^{2-} ions existing in the reaction solution around the ZnSe flower-like nanostructures because of the dynamical equilibrium reaction 1. When the Cu^{2+} ions are added into the suspension of ZnSe, CuSe preferentially in situ deposits on the surface of ZnSe flower-like nanostructures by heterogonous nucleation based on reaction (2), which results in the formation of CuSe-ZnSe flower-like nanocomposite. So it is not surprising that the content of CuSe clusters can be increased obviously with increasing the amount of added Cu^{2+} ions. Due to the relatively low amount of Cu^{2+} ions, the flower-like nanostructure may be still maintained well in the obtained nanocomposites.

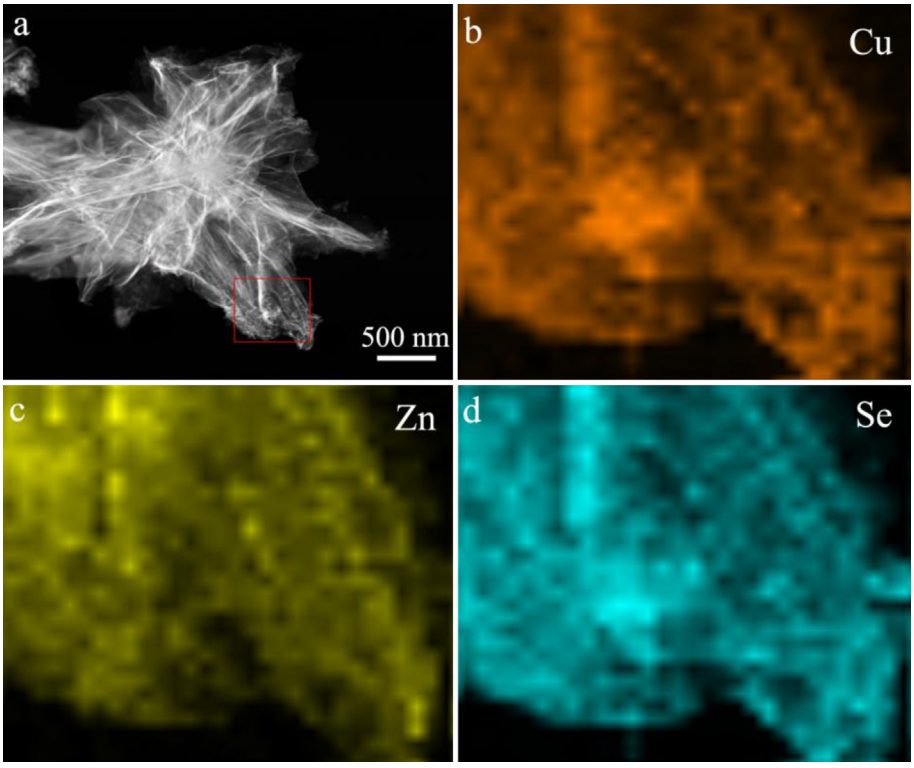

Fig. 4. STEM images of the sample 4: (a) a typical CuSe-ZnSe flower-like nanocomposite, (b) Cu element, (c) Zn element and (d) Se element.

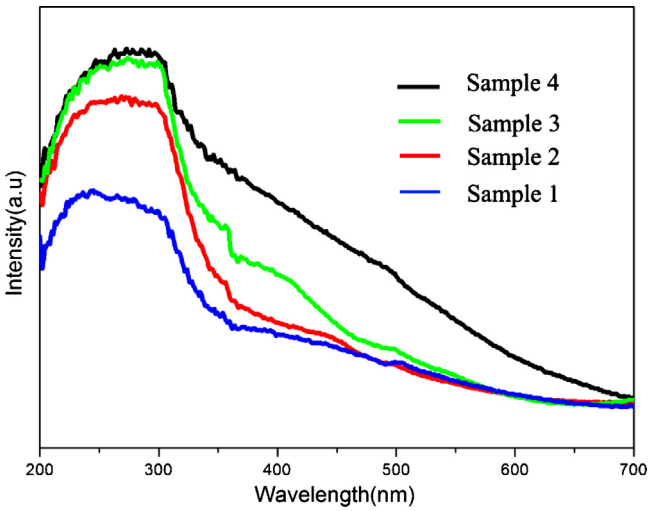

Fig. 5. UV–visible absorption spectra of samples 1–4.

Fig. 5 displays the comparison of UV–visible absorption spectra of samples 1–4. The band gap of sample 1 (pure ZnSe nanoflowers) estimated from the main absorption edges of the spectrum is 2.8 eV, which is slightly higher that the well-known band gap of 2.7 eV for bulk ZnSe due to the so-called "quantum size effect". All of the CuSe-ZnSe flower-like nanocomposites (sample 2–4) show clearly strong absorption in the wider visible region (ca. 350–600 nm). It is also observed that the absorption intensity increase with the growing amount of CuSe content in the CuSe-ZnSe nanocomposites, according to the progressively intensive browning of the samples (from light yellow to brown). These results demonstrate that the ZnSe flower-like nanostructures can be successfully sensitized by CuSe particles.

The photocatalytic degradation behaviors of organic dyes (methylene blue (MB) and methyl orange (MO)) by as-obtained ZnSe flower-like nanostructures (sample 1) and CuSe-ZnSe flower-like nanocomposites (sample 2–4) under visible irradiation (≥420 nm) are shown in Fig. 6. Before the photocatalytic reaction, these organic dye solutions were first photolyzed in the absence of the photocatalysts to examine their stability. The results show that the organic dyes are not decomposed, even after long illumination with visible irradiation. In addition, the concentrations of dyes almost do not change under dark conditions after these ZnSe-based photocatalysts and organic dye solutions reach the adsorption-desorption equilibrium. Therefore, the presence of both ZnSe-based photocatalysts and illumination is necessary for efficient degradation. Fig. 6a and c show the UV–vis absorption spectra of an aqueous solution of the two dyes (initial concentration: 1.0×10^{-4} M, 100 mL) in the presence of as-prepared sample 4 under exposure to the 300 W xenon lamp for various durations, respectively. The characteristic absorption of the MO at $\lambda = 465$ nm and MB at $\lambda = 656$ nm is chosen to monitor the photocatalytic degradation process, respectively. The characteristic absorption of the MO and MB can be observed to almost disappear after 90 min and 60 min, respectively. These results exhibit the CuSe-ZnSe flower-like nanocomposites possessed the excellent photocatalytic degradation activity of organic dyes under visible irradiation. Figure 6b and 6d show the MO and MB degradation ratio (DR) of the sample 1–4 under visible irradiation, respectively. Sample 4 reach the maximum DR of both MO (ca. 100%, 90 min) and MB (ca. 96%, 60 min), which are over 4 times and 2.5 times than sample 1 (pure ZnSe flower-like nanostructures), respectively. In addition, the DR of CuSe-ZnSe flower-like nanocomposites for both MO and MB are increased congruously with the growing amount

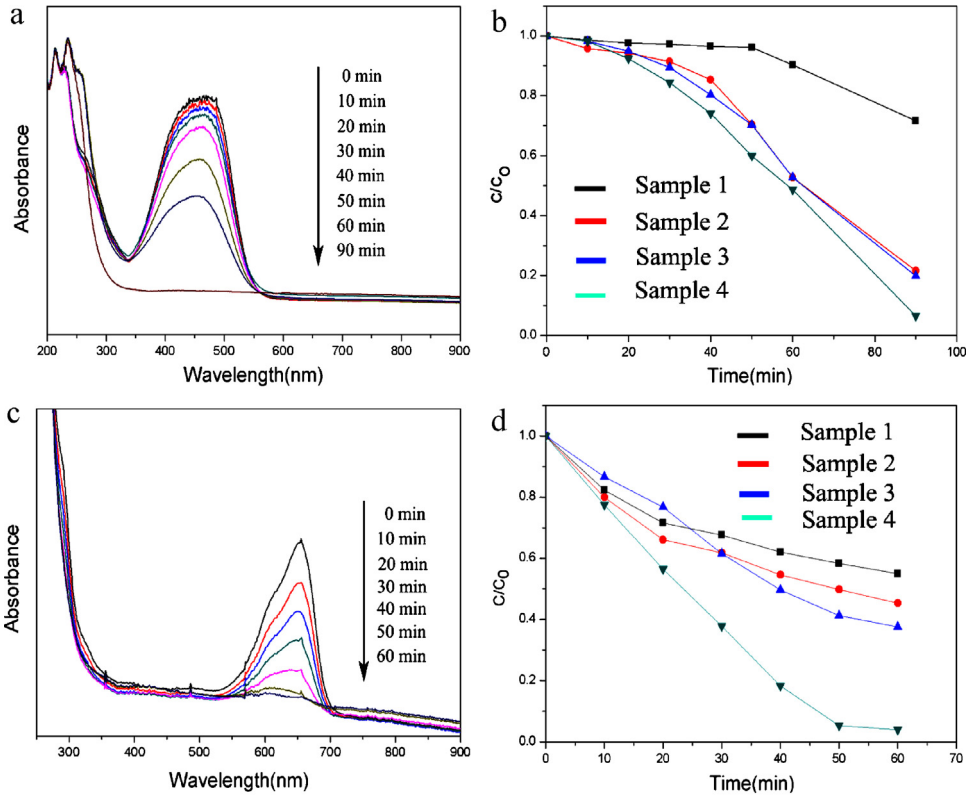

Fig. 6. Absorption spectrum of (a) methyl orange and (c) methylene blue in the presence of sample 4 under the irradiation of visible light (≥420 nm). Comparison of photocatalytic activities of samples 1–4 for the photocatalytic degradation of (b) methyl orange and (d) methylene blue under the irradiation of visible light (≥420 nm).

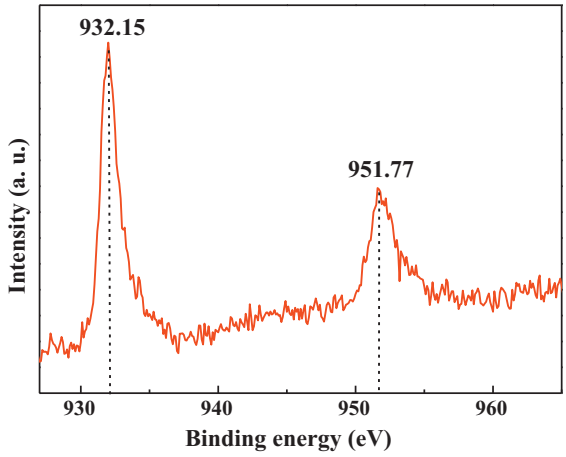

Fig. 7. The Cu 2p region in XPS spectrum of samples 4 after photocatalytic reaction for 1.5 h.

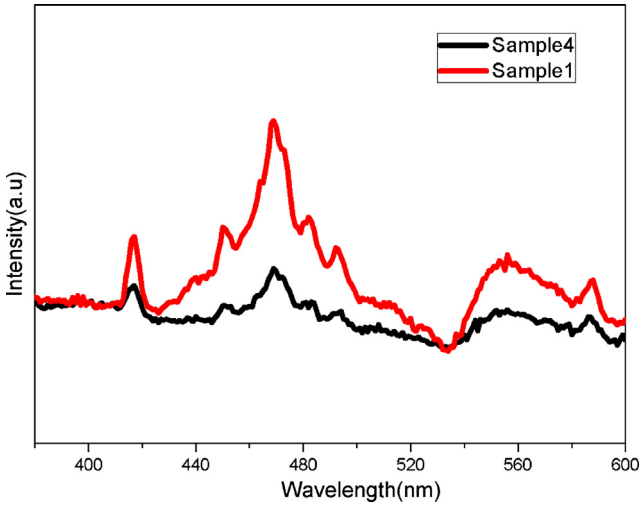

Fig. 8. PL spectra of sample 1 and 4 (λ_{ex} = 320 nm).

of CuSe content. Compare with all previous reports on the photocatalytic degradation behaviors of ZnSe-based photocatalysts for MO, CuSe-ZnSe flower-like nanocomposites (especially sample 4) we obtained also exhibit the highest photocatalytic degradation activity under visible irradiation [16,24].

In some recent reports on Cu(II)/TiO_2 nanocomposites, the visible light initiates interfacial charge transfer (IFCT) mechanism for explaining the enhanced photocatalytic activity was proposed. Under the effect of this mechanism, electrons in the valence band (VB) of TiO_2 are transferred directly to Cu(II), forming Cu(I). The holes produced in the VB are then capable of decomposing organic substances [44–46]. Very recently, Yu et al. also developed the visible-light-driven CuS/ZnS porous nanosheets photocatalysts with high H_2 production activity based on the IFCT mechanism [39]. In our case, we propose that the visible light irradiation induces IFCT from the VB of ZnSe to CuSe clusters. The enhanced UV–vis absorption from 350 to 600 nm (Fig. 5) provides the direct evidence. In addition, the XPS results (Fig. 7) of samples 4 after photocatalytic reaction for 1.5 h can also confirm that the transferred electrons from the VB of ZnSe to CuSe cause the partial reduction of CuSe to Cu_2Se. Two shakeup line almost disappear and the binding energies of Cu $2p_{3/2}$ and Cu $2p_{1/2}$ slightly left-shift to 932.15 eV and 951.77 eV, respectively, which indicates the presence of Cu (I). According the Nernst equation, the potential of CuSe/Cu_2Se can be calculated as follow: $\varphi^{\theta}_{CuSe/Cu_2Se} = \varphi^{\theta}_{Cu_2^+/Cu^+} + 0.059/2\, lg\,(K^{\theta}_{sp}CuSe/K^{\theta}_{sp}\,Cu_2Se = -0.53$ V. The band edge positions of the CB and VB of ZnSe can be determined by the following equation: $E_{CB} = \chi - E^e - 1/2E_g$, where E_{CB} is the conduction band edge potential, χ is the electronegativity of the semiconductor, expressed as the geometric mean of the absolute electronegativity of the constituent atoms. E^e is the energy of free electrons on the hydrogen scale ca. 4.5 eV. E_g is the bandgap of the semiconductor. The calculated conduction and valence band positions of ZnSe prepared in our experimental condition at the point of zero are about −0.64 eV and 2.16 eV, respectively. So the interfacial transition energy from the VB of ZnSe to CuSe/Cu2Se is determined to be 2.27 eV. Further it is reasonable to assume that the absorption from 350 to 600 nm can be ascribed to the direct IFCT from the VB of ZnSe to CuSe. Fig. 8 shows the photoluminescence (PL) spectra of sample 1 and 4. Before the measurement, samples (10 mg) were firstly well dispersed into 5 ml ethanol. The measurement was conducted at the excitation wavelength of 320 nm with PMT voltage of 500 V. From the PL spectra results, we can easily conclude that the PL emission intensity of sample 4 is weaker than the sample 1. It is well known that the PL emission intensity of a semiconductor is proportional to the opportunity for the recombination of photo-induced electron–hole pairs. In other words, this can prove that the CuSe-ZnSe flower-like nanocomposites under the effect of IFCT has lesser opportunity of electron–hole pairs' recombination and facilitates the migration of electrons more effectively than the pure ZnSe nanostructures. To the best of our knowledge, this is the first time that the ion-exchange preparation and enhanced photocatalytic activity of selenides flower-like nanocomposites have been reported. We believe that the prepared CuSe-ZnSe flower-like nanocomposites are also of great interest in solar cells, catalysis, separation technology, biomedical engineering, and nanotechnology.

Based on the above results, a tentative mechanism of photocatalytic degradation process for MO and MB on the CuSe-ZnSe flower-like nanocomposites can be drawn (Fig. 9). When illuminated by visible light, the transferred electrons from VB of ZnSe to CuSe clusters cause the partial reduction of CuSe to Cu_2Se (Eq. (1–2)). These CuSe/Cu_2Se cluster can act as an electron sink and co-catalyst to promote the separation and transfer of photo-generated electrons from the VB of ZnSe to the CuSe/Cu_2Se cluster, which obstructs effectively the recombination process of electron–hole pairs in ZnSe. After the electrons transfer into CuSe cluster, an excess of holes are left on the irradiated ZnSe. According to the location of the VB (2.16 eV) of obtained ZnSe-CuSe nanoflowers and the normal potential of $OH^-/{}^{\bullet}OH$ couples (above 2.2 eV vs SCE)

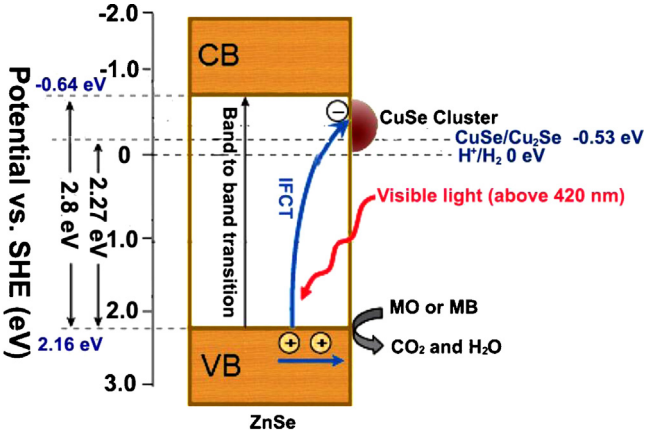

Fig. 9. The mechanism of photocatalytic degradation process for MO and MB of the obtained CuSe-ZnSe flower-like nanocomposites under visible light.

[47–49], the photogenerated holes could not react with OH^-/H_2O to produce •OH. So the direct reaction between photo-generated holes and adsorbed organic dyes may be considered as a way of oxidation on ZnSe (Eq. (3)). According to this proposed route, the final products of dyes oxidation, CO_2 and H_2O, are formed through a series of possible reactions. Thus, it is not surprising that when more CuSe clusters are deposited on the surface of ZnSe nanoflowers with increasing Cu content, the photocatalytic degradation activity under visible irradiation are enhanced obviously due to more IFCT electrons produced. In this case, we only focus on the effect of charge transfer process to the photocatalytic activity of the as-prepared photocatalysts, the complex reaction mechanism for the photo-degradation process of organic dyes is not quite clear.

$$ZnSe/CuSe + hv \rightarrow ZnSe(h^+)/CuSe(e^-) \quad (1)$$

$$2CuSe + e^- \rightarrow 2Cu_2Se + Se^{2-} \quad (2)$$

$$h^+ + MOorMB \rightarrow CO_2 + H_2O \quad (3)$$

4. Conclusion

In summary, CuSe-ZnSe flower-like nanocomposites with uniform diameters can be easily fabricated on a large scale by a controlled ion-exchange reaction between monodisperse ZnSe flower-like nanostructures and Cu^{2+} ions in solution. The difference of solubility products (K_{sp}) of ZnSe and CuSe is the main driving force for the formation of these flower-like nanocomposites. The Cu content greatly influences the physical properties and photocatalytic activity of obtained CuSe-ZnSe nanocomposites. The as-produced CuSe-ZnSe nanocomposites show tremendous enhancements on the photocatalytic degradation ratio of organic dyes MO and MB under visible-light irradiation. The 8 wt.% CuSe-ZnSe sample exhibits the highest degradation ratio for both MO (ca. 100%, 90 min) and MB (ca. 96%, 60 min), which are over 4 times and 2.5 times than that of the pure ZnSe sample, respectively. Based on the data of UV–vis diffuse reflection spectra, XPS and PL spectra, the enhancements of photocatalytic activities of CuSe-ZnSe flower-like nanocomposites are due to the effective separation of photo-electrons and holes induces by the direct IFCT from the VB of ZnSe to CuSe, which results in the reduction of CuSe to Cu_2Se. This work not only highlights the potential use of visible-light-driven CuSe-ZnSe flower-like nanocomposites photocatalysts, but also emphasizes the simple ion-exchange in situ growth method for the preparation of selenides heterogeneous structures.

Acknowledgment

We gratefully acknowledge the financial support of National Natural Science Foundation of China (No.21001086 and 21276116), Postgraduate Research Foundation of Jiangsu Province (No.1102123C), National Postgraduate Research Foundation of China (No.2011M500853), Science Department of Jiangsu Province (No.BK2010340) and Jiangsu University (No.10JDG070).

References

[1] A. Fujishima, K. Honda, Nature 37 (1972) 238.
[2] M. Anpo, M. Takeuchi, Journal of Catalysis 216 (2003) 505.
[3] M.A. Fox, M.T. Dulay, Chemical Reviews 93 (1993) 341.
[4] M.R. Hoffman, S.T. Martin, W. Choi, Chemical Reviews 95 (1995) 69.
[5] L.S. Zhang, K.H. Wong, Z.G. Chen, J.C. Yu, J.C. Zhao, C. Hu, C.Y. Chan, P.K. Wong, Applied Catalysis A – General 363 (2009) 221.
[6] M. Kemell, V. Pore, M. Ritala, M. Leskela, M. Linden, Journal of the American Chemical Society 127 (2005) 14178.
[7] C.Z. Wu, L.Y. Lei, X. Zhu, J.L. Yang, Y. Xie, Small 3 (2007) 1518.
[8] C.C. Kim, S. Sivananthan, Physical Review B 53 (1996) 1475.
[9] H. Yu, J. Li, R.A. Loomis, P.C. Gibbons, L.W. Wang, W.E. Buhro, Journal of the American Chemical Society 125 (2003) 16168.
[10] Y.W. Jun, J.E. Koo, J. Cheon, Chemical Communications (2000) 1243.
[11] H.R. Heulings-IV, X.Y. Huang, J. Li, Nano Letters 1 (2001) 521.
[12] H. Fujiwara, H. Hosokawa, K. Murakoshi, Y. Wada, S. Yanagida, T. Okada, H. Kobayashi, Journal of Physical Chemistry B 102 (1998) 4440.
[13] Z. Wang, C.J. Medforth, J.A. Shelnutt, Journal of the American Chemical Society 126 (2004) 16720.
[14] S.L. Xiong, B.J. Xi, C.M. Wang, G.F. Zou, L.F. Fei, W.Z. Wang, Y.T. Qian, Chemistry – A European Journal 13 (2007) 7926.
[15] F. Cao, W.D. Shi, L.J. Zhao, S.Y. Song, J.H. Yang, Y.Q. Lei, H.J. Zhang, Journal of Physical Chemistry C 112 (2008) 17095.
[16] Y. Zhang, C.G. Hu, B. Feng, X. Wang, B.Y. Wan, Applied Surface Science 257 (2011) 10679.
[17] S.L. Xiong, J.M. shen, Q. Xie, Y.Q. Gao, Q. Tang, Y.T. Qian, Advanced Functional Materials 15 (2005) 1787.
[18] B. Xiang, H.Z. Hang, G.H. Li, F.H. Su, R.M. Wang, J. Xu, G.W. Lu, X.C. Xun, Q. Zhao, D.P. Yu, Applied Physics Letters 82 (2003) 3330.
[19] C.R. Wang, J. Wang, Q. Li, G.C. Yi, Advanced Functional Materials 15 (2005) 1471.
[20] S.H. Kang, W. Lee, H.S. Kim, Materials Letters 85 (2012) 74.
[21] P.D. Cozzoli, L. Manna, M.L. Curri, S. Kudera, C. Giannini, M. Striccoli, A. Agostiano, Chemistry of Materials 17 (2005) 1296.
[22] M.Q. He, D. Li, D.L. Jiang, M. Chen, Journal of Solid State Chemistry 192 (2012) 139.
[23] C.W. Lai, S. Sreekantan, W. Krengvirat, Electrochimica Acta 77 (2012) 12.
[24] P. Chen, T.Y. Xiao, H.H. Li, J.J. Yang, Z. Wang, H.B. Yao, S.H. Yu, ACS Nano 6 (2012) 712.
[25] V.M. Bhuse, P.P. Hankare, K.M. Garadkar, A.S. Khomane, Materials Chemistry and Physics 80 (2003) 82.
[26] H. Okimura, T. Matsumae, R. Makabe, Thin Solid Films 71 (1980) 53.
[27] W.S. Chen, J.M. Stewart, R.A. Mickelsen, Applied Physics Letters 46 (1985) 1095.
[28] R.C. Kainthla, D.K. Pandya, K.L. Chopra, Journal of the Electrochemical Society 127 (1980) 277.
[29] S.T. Lakshmikvmar, Solar Energy Materials & Solar Cells 32 (1994) 7.
[30] C. Levy-Clement, M. Neumann-Spallart, S.S. Haram, K.S.V. Santhanam, Thin Solid Films 302 (1997) 12.
[31] P.P. Hankare, A.S. Khomane, P.A. Chate, K.C. Rathod, K.M. Garadkar, Journal of Alloys and Compounds 469 (2009) 478.
[32] P. Kumar, K. Singh, O.N. Srivastava, Journal of Crystal Growth 312 (2010) 2804.
[33] G. Statkute, I. Mikulskas, A. Jagminas, Optical Materials 30 (2008) 743.
[34] A. Jagminas, R. Juskenas, I. Gailiute, G. Statkute, R. Tomasiunas, Journal of Crystal Growth 294 (2006) 343.
[35] Y. Zhang, C.G. Hu, C.H. Zheng, Y. Xi, B.Y. Wan, Journal of Physical Chemistry C 114 (2010) 14849.
[36] R. Yu, T. Ren, K.J. Sun, Z.C. Feng, G.N. Li, C. Li, Journal of Physical Chemistry C 113 (2009) 10833.
[37] J. Choi, N. Kang, H.Y. Yang, H.J. Kim, S.U. Son, Chemistry of Materials 22 (2010) 3586.
[38] J.G. Yu, J. Zhang, S.W. Liu, Journal of Physical Chemistry C 114 (2010) 13642.
[39] J. Zhang, J.G. Yu, Y.M. Zhang, Q. Li, J.R. Gong, Nano Letters 11 (2011) 4774.
[40] F. Zhang, D.Y. Zhao, ACS Nano 3 (2009) 159.
[41] L. Dloczik, R. Koenenkamp, Journal of Solid State Electrochemistry 8 (2004) 142.
[42] Y.F. Yu, J. Zhang, X. Wu, W.W. Zhao, B. Zhang, Angewandte Chemie International Edition 51 (2012) 897.
[43] C.D. Wagner, W.W. Riggs, L.E. Davis, J.F. Moulder, G.E. Muilenberg, Handbook of X-ray Photoelectron Spectroscopy, PerkinElmer, Eden Prairie, MN, 1978.
[44] X.Q. Qiu, M. Miyauchi, H.G. Yu, H. Irie, K. Hashimoto, Journal of the American Chemical Society 132 (2010) 15259.
[45] H. Irie, S. Miura, K. Kamiya, K. Hashimoto, Chemical Physics Letters 457 (2008) 202.
[46] H. Irie, K. Kamiya, T. Shibanuma, S. Miura, D.A. Tryk, T. Yokoyama, K. Hashimoto, Journal of Chemical Physics 113 (2009) 10761.
[47] J.G. Yu, X.X. Yu, Environmental Science and Technology 42 (2008) 4902.
[48] F.R.F. Fan, P. Leempoel, A.J. Bard, Journal of the Electrochemical Society 130 (1983) 1866.
[49] Y.I. Kim, S.J. Atherton, E.S. Brigham, T.E. Mallouk, Journal of Physical Chemistry 97 (1993) 11802.